Frontiers in Bioscience Landmark

Front. Biosci. (Landmark Ed) **2024**; 29(12): 428
https://doi.org/10.31083/j.fbl2912428

Original Research

Effect of 2-Aminoethoxydiphenyl Borate on the State of Skeletal Muscles in Dystrophin-Deficient *mdx* Mice

Mikhail V. Dubinin[1,*], Anastasia E. Stepanova[1], Anastasia D. Igoshkina[1], Irina B. Mikheeva[2], Eugeny Yu. Talanov[3], Alena A. Cherepanova[1], Konstantin N. Belosludtsev[1,3]

[1]Department of Biochemistry, Cell Biology and Microbiology, Mari State University, 424001 Yoshkar-Ola, Russia
[2]Laboratory of Experimental Neurobiology, Institute of Theoretical and Experimental Biophysics, Russian Academy of Sciences, 142290 Pushchino, Russia
[3]Laboratory of Mitochondrial Transport, Institute of Theoretical and Experimental Biophysics, Russian Academy of Sciences, 142290 Pushchino, Russia
*Correspondence: dubinin1989@gmail.com (Mikhail V. Dubinin)

Academic Editor: Ioanna-Katerina Aggeli
Submitted: 6 August 2024 Revised: 10 November 2024 Accepted: 20 November 2024 Published: 25 December 2024

Abstract

Objective: Ca^{2+} overload of muscle fibers is one of the factors that secondarily aggravate the development of Duchenne muscular dystrophy (DMD). The purpose of this study is to evaluate the effects of the Ca^{2+} channel modulator 2-aminoethoxydiphenyl borate (APB) on skeletal muscle pathology in dystrophin-deficient *mdx* mice. **Methods**: Mice were randomly divided into six groups: wild type (WT), WT+3 mg/kg APB, WT+10 mg/kg APB, *mdx*, *mdx*+3 mg/kg APB, *mdx*+10 mg/kg APB. APB was administered intraperitoneally daily for 28 days. Finally, we assessed the grip strength and hanging time of mice, the histology and ultrastructure of the quadriceps, as well as the parameters reflecting quadricep mitochondrial function. **Results**: 3 mg/kg APB was shown to reduce creatine kinase activity in the serum, intensity of degeneration and the level of fibrosis in the quadriceps of *mdx* mice, and improved tissue ultrastructure. However, this effect of APB was not sufficient to improve grip strength and hanging time of *mdx* mice. The effect of 3 mg/kg APB may be due to improve Ca^{2+} homeostasis in skeletal muscles, as evidenced by a trend toward decreased Ca^{2+} overload of quadricep mitochondria. High dose of APB (10 mg/kg body weight) showed less pronounced effect on the pathological phenotype of *mdx* mice. Moreover, 10 mg/kg APB disrupted the ultrastructure of the quadriceps and caused a decrease in grip strength in WT mice. **Conclusions**: APB is able to improve the phenotype in *mdx* mouse DMD model. However, the effect of APB is quite limited, which may be due to its multitargeting of Ca^{2+} channels in the membranes of muscle fibers and intracellular organelles, differentially expressed in DMD.

Keywords: 2-aminoethoxydiphenyl borate; Duchenne muscular dystrophy; *mdx* mice; skeletal muscles; mitochondria; calcium

1. Introduction

Duchenne muscular dystrophy (DMD) is the most common X-linked recessive inherited muscle disorder, affecting one in 3500 to 5000 males [1,2]. The disease is caused by various mutations in the *DMD* gene, resulting in the loss of the dystrophin protein, which plays an important role in the formation of the dystrophin-associated protein complex (DAPC) that structurally links the sarcolemma, cytoskeleton and extracellular matrix [2]. This leads to the disassembly of DAPC and, as a consequence, to the disruption of membrane integrity during muscle contraction and relaxation cycles and eventually to the death of muscle fibers.

Numerous studies on human biopsies and animal models, in particular dystrophin-deficient *mdx* mice, demonstrate a chronic increase in Ca^{2+} levels in dystrophin-deficient muscles, which is primarily due to excessive Ca^{2+} influx from the extracellular matrix through membrane ruptures, as well as due to abnormal activity of sarcolemmal channels [2–4]. These events lead to overactivation of Ca^{2+}-dependent proteases and proteolysis, oxidative stress and muscle fiber necrosis. DMD is also accompanied by disrupted sarcoplasmic reticulum (SR) Ca^{2+} handling and, along with this, excessive Ca^{2+} overload of mitochondria, resulting in mitochondrial dysfunction, causing a decrease in the efficiency of ATP synthesis, overproduction of reactive oxygen species (ROS) and the opening of the mitochondrial permeability transition (MPT) pore mediating cell death [2–4].

There are various approaches aimed at improving Ca^{2+} homeostasis in dystrophin-deficient muscle fibers and based on modulation of Ca^{2+} channels of the muscle fiber membrane (transient receptor potential channels (TRPC), voltage-gated calcium (Ca_V) channels, store-operated calcium entry (SOCE) channels and others), sarcoplasmic reticulum (sarco/endoplasmic reticulum Ca^{2+}-ATPase (SERCA), inositol-1,4,5-triphosphate receptor (IP_3R) and ryanodine receptor (RyR)), and mitochondria (MPT pore components) [3–5]. This often involves the use of target-specific pharmacological modulators, whose combination can lead to numerous side effects in the body. For this reason, it is necessary to create universal agents capable of

modulating the activity of a number of calcium channels and Ca^{2+} buffering systems.

Universal ion channel modulators include amphiphilic boron chemicals, such as 2-aminoethoxydiphenyl borate (APB), which, due to its structure, is able to modulate various ion channels. It was initially used as an inhibitor of IP_3R [6], but is now also known as an inhibitor of SERCA [7–9], SOCE channels (stromal interaction molecule 1/Orai1) [10–12], TRPC1/3/4/6/7 and transient receptor potential melastatin channels [13–16]. Moreover, APB is also considered as an inhibitor of mitochondrial calcium transport systems [17–19]. At the same time, APB has been shown to activate transient receptor potential vanilloid (TRPV) type 1–4 and TRPV6 channels [20–23]. APB is thought to exert a dose-dependent bimodal effect on these transporters. In particular, the bimodal effect of APB on SOCE is best known. Experiments in cell cultures show that low doses of APB enhance SOCE and large doses inhibit this process [10]. This APB-induced modulation of cellular ion channels has beneficial effects in various *in vivo* neurodegenerative and ischemic injury models [18,24–27]. In the context of DMD, APB-induced inhibition of overactivated IP_3R pathways in the SR has previously been shown to reduce Ca^{2+} overload in cultured dystrophin-deficient myotubes, increasing cell viability [28]. However, the effect of APB administration on dystrophin-deficient animal models is still unknown.

In this study, we evaluated for the first time *in vivo* the effect of APB on the ultrastructure of dystrophin-deficient skeletal muscles of *mdx* mice, as well as the main indicators reflecting the severity of skeletal muscle pathology in these animals, including mitochondrial dysfunction associated with Ca^{2+} overload. In addition, we assessed the effect of APB on the ultrastructure and state of skeletal muscles of healthy C57BL10 strain mice (wild type, WT). We found that low dose APB (3 mg/kg/day) tended to improve some parameters in *mdx* mice, but high dose (10 mg/kg/day) had little effect on skeletal muscle health in *mdx* mice and exhibited negative effects in wild-type animals, possibly due to the known multiple targets of this agent in skeletal muscle.

2. Materials and Methods

2.1 Experimental Animals

Male mice of the C57BL10 mice (wild type, WT) and dystrophin-deficient C57BL/10ScSn-*mdx* (*mdx* mice) were from the Russian Academy of Sciences' Shemyakin and Ovchinnikov Institute of Bioorganic Chemistry (Biomodel, Pushchino, Russia). The following groups were used in this experiment: (1) WT mice treated with vehicle (WT, $n = 10$); (2) WT mice treated with 3 mg/kg APB (WT+APB 3, $n = 7$); (3) WT mice treated with 10 mg/kg APB (WT+APB 10, $n = 9$); (4) *mdx* mice treated with vehicle (*mdx*, $n = 10$); (5) *mdx* mice treated with 3 mg/kg APB (*mdx*+APB 3, $n = 7$); (6) *mdx* mice treated with 10 mg/kg APB (*mdx*+APB 10, $n = 9$). Treatment of all mice began at 8 weeks of age. Fresh APB (Sigma-Aldrich, St. Louis, MO, USA) solution in 5% DMSO in saline was administered intraperitoneally (150–170 µL per animal) daily for 4 weeks. Control WT and *mdx* mice received vehicle (5% DMSO in saline). At the end of the treatment period, the mice were sacrificed by cervical dislocation under anesthesia with zoletil (Valdepharm, Val-de-Reuil, France)/xylazine (Bioveta, Ivanovice na Hane, Czech Republic) mixture. The blood was collected in 1.5-mL Eppendorf tubes and left to coagulate at room temperature and centrifuged at 800 ×g at 4 °C for 10 min. The resulting serum was stored at –80 °C for further analysis. Fresh samples of the quadriceps (*vastus lateralis*) were taken for subsequent histological and electron microscopic analysis. Fresh samples of skeletal muscle tissue (total quadriceps of both legs) were used for mitochondrial isolation.

2.2 Muscle Strength and Endurance Testing

The muscle strength of the animals evaluated using the grip strength test (IITC Life Science, Woodland Hills, CA, USA). Mice were familiarized with the test one week before sacrifice. Final testing was performed the day before sacrifice. The results were presented as grams/animal body weight. The average of three trials from each mouse was used for analysis.

The endurance of mice was determined using a wire-hanging test. Mice were familiarized with the test one week before sacrifice. Final testing was performed the day before sacrifice (one hour after the grip strength test, in the same sequence of animals). The testing was performed on a setup consisting of a 3-mm thread string (38 cm long and 49 cm above the padded surface). The maximum wire-hanging time was used to reflect endurance. Holding impulse (s × g) = hanging time (s) × body weight (g) was used to correct for the negative effects of body weight on the hanging time, and reflected the minimal amount of sustained tension (impulse) that a mouse developed for supporting itself on the bar against gravity for a given time [29].

2.3 Creatine Kinase, Aspartate Aminotransferase (AST) and Lactate Dehydrogenase (LDH) Assays

Creatine kinase, AST and LDH activities in mouse serum were analyzed at 340 nm using commercially available kits (Vector-Best, Novosibirsk, Russia) and a Multiscan Go plate reader (Thermo Fisher Scientific, Waltham, MA, USA).

2.4 Histological Analysis

Mouse quadriceps (*vastus lateralis*, five samples/group from random animals) were embedded in paraffin after pre-treatment as described previously [30]. The blocks were then sectioned into 5 µm serial sections using a Minux S710 rotary microtome (RWD, Shenzhen, China). The resulting slides were stained with hematoxylin

and eosin (H&E) to estimate the severity of histological changes and with Sirius red to assess the level of fibrosis. Images (muscle mid-belly region defined as shown earlier [31]) were evaluated using the EVOS M5000 microscope (Thermo Fisher Scientific, Waltham, MA, USA). Pictures were taken in transmitted light channel and further analyzed using ImageJ software version 1.53 (National Institutes of Health, Bethesda, MD, USA). Degenerative fibers (showing loss of striation/homogeneous appearance of fiber content) and regenerative fibers (having basophilic cytoplasm, large peripheral or central nuclei with prominent nucleoli), as well as inflammatory foci per field were scored in five high-power (40×) non-overlapping fields in a blinded manner as described previously [32]. The same fields were observed to measure the minimal Feret's diameter using the XP-Pen graphic tablet (XP-PEN, Shenzhen, China) and freehand selection tool of the Image J software. The area of connective tissue (fibrosis) was quantified using the XP-Pen graphic tablet (XP-PEN) and freehand selection tool of the Image J software and expressed as a percentage of the area of tissue stained with Sirius red to the total area of the section. The average from each mouse (at least 10 serial sections per animal) was included in the analysis.

2.5 Transmission Electron Microscopy

Mouse quadriceps (*vastus lateralis*, three samples per group from random animals, whose tissue was also collected for histology) were processed as described previously [33]. Briefly, semi-thin sections were first obtained to determine the mid-belly region and the transverse orientation of the muscle (according to [31]) using the EVOS M5000 microscope (Thermo Fisher Scientific). Samples from the solid epon blocks were sectioned into 60–70 nm ultrathin sections using a Leica EM UC6 ultramicrotome (Leica, Wetzlar, Germany) and then counterstained with uranyl acetate and lead citrate. JEM-1400 (JEOL, Tokyo, Japan) electron microscope was used to image the samples. The images were analyzed using ImageJ 1.53c (National Institutes of Health, Bethesda, MD, USA). Morphometric analysis of mitochondria was performed by manual contouring of cross sections of organelles along their outer membrane and mitochondria-associated membranes (mitochondria-associated membranes (MAM) contacts) within 30 nm [34]. 150 cross-sectional profiles of mitochondria (50 profiles/sample) were collected for each group of mice. The average from each mouse was included in the analysis.

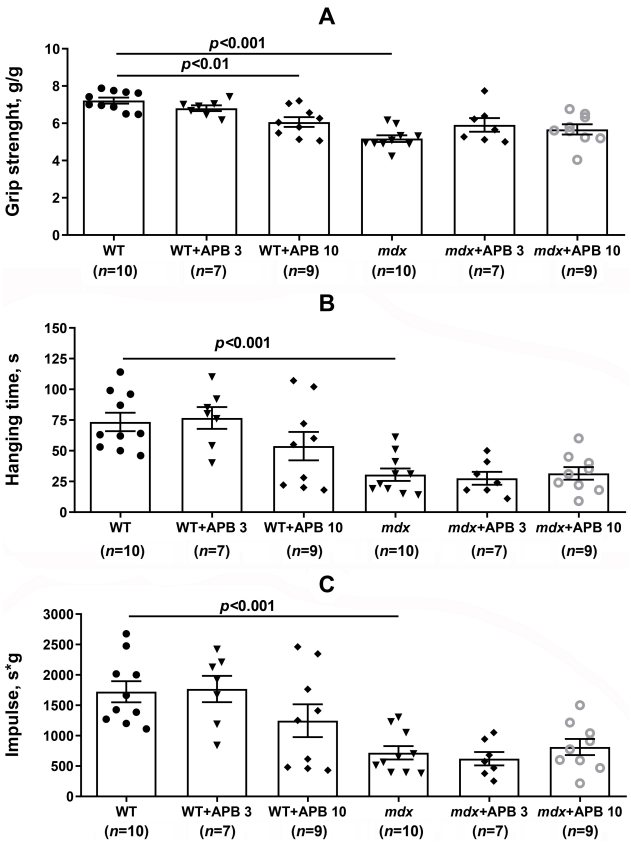

Fig. 1. The effect of 3 mg/kg or 10 mg/kg 2-aminoethoxydiphenyl borate (APB) on mouse muscle strength and endurance. (A) Grip strength. (B) Wire-hanging time. (C) The holding impulse. Data are expressed as mean ± SEM. WT, wild type.

Table 1. Comparison of histological parameters in quadriceps muscle.

Measurement	WT	WT+APB 3	WT+APB 10	*mdx*	*mdx*+APB 3	*mdx*+APB 10
Number of fibers/field	57.73 ± 6.93	72.20 ± 7.93	69.07 ± 14.58	93.69 ± 12.38	53.19 ± 8.99	81.17 ± 5.87
Central nuclei/field	0.58 ± 0.17	0.90 ± 0.21	0.82 ± 0.14	69.43 ± 12.27*	43.28 ± 6.85*$^{\#}$	67.22 ± 4.63*
Peripheral nuclei/field	76.40 ± 9.64	92.81 ± 4.96	92.22 ± 10.20	111.14 ± 16.27	56.91 ± 6.29$^{\#}$	103.05 ± 5.05$^{\gamma}$
Number of fibers with centralized nuclei/field	0.85 ± 0.43	1.10 ± 0.38	1.08 ± 0.41	49.31 ± 5.93*	23.10 ± 2.91*$^{\#}$	40.48 ± 2.97$^{\gamma}$
Degenerating fibers/field	1.57 ± 0.52	1.51 ± 0.56	2.87 ± 0.67	42.24 ± 2.64*	12.75 ± 1.23*$^{\#}$	23.35 ± 2.52 *$^{\#\gamma}$
Regenerating fibers/field	1.17 ± 0.59	0.73 ± 0.35	1.53 ± 0.35	9.44 ± 3.33*	10.44 ± 1.78*	18.18 ± 1.92*$^{\#\gamma}$
Inflammatory foci/field	0.13 ± 0.09	0.12 ± 0.06	0.77 ± 0.20	2.74 ± 0.38*	0.93 ± 0.11*$^{\#}$	1.43 ± 0.23*$^{\#}$

Data were collected from 5 non-overlapping field from each sample and average of all samples within a group (mean ± SEM, $n = 5$). * $p < 0.05$ versus WT group, $^{\#}$ $p < 0.05$ versus *mdx* group, $^{\gamma}$ $p < 0.05$ versus *mdx*+APB 3 group.

2.6 Isolation of Skeletal Muscle Mitochondria and Analysis

The quadriceps muscles of both legs (4–6 samples/group from random animals) were used to isolate mitochondria by differential centrifugation [35]. The final mitochondrial suspension contained approximately 20–30 mg mitochondrial protein/mL (determined by Bradford assay). Mitochondrial O_2 consumption was monitored using the Oxygraph Plus system (Hansatech Instruments, King's Lynn, UK). The respiratory buffer contained 120 mM KCl, 5 mM NaH_2PO_4, 2.5 mM K-glutamate, 2.5 mM K-malate, 10 mM HEPES-KOH (pH 7.4). O_2 consumption measurements consisted of sequential addition of 200 µM ADP and 50 µM 2,4-dinitrophenol (DNP) to an oxygen chamber containing 0.25 mg mitochondrial protein/mL in the incubation medium. The O_2 consumption rate was expressed as nmol O_2/min/mg mitochondrial protein. The respiratory control ratio (RCR = state 3/state 4) was used as a quantitative indicator of mitochondrial quality [36].

Lipid peroxidation in mitochondria was quantified by the level of thiobarbituric acid-reactive substances (TBARS, mainly malondialdehyde (MDA)) using a commercially available kit (Agat-Med, Moscow, Russia).

Mitochondrial Ca^{2+} transport was monitored using the arsenazo III Ca^{2+} probe (at 675 and 685 nm) and a Multiscan Go reader (Thermo Fisher Scientific, Waltham, MA, USA) [33]. To quantify the free matrix calcium, 2 mg mitochondrial protein/mL were resuspended in 210 mM mannitol, 70 mM sucrose, 2.5 mM K-glutamate, 2.5 mM K-malate, 1 mM KH_2PO_4, 10 µM EGTA, 10 mM HEPES-KOH buffer (pH 7.4.) and supplemented with 50 µM arsenazo III. 0.1 mg/mL alamethicin (ALM) was added to induce nonspecific permeability of mitochondrial membranes and Ca^{2+} release accompanied by a sharp increase in arsenazo III absorption [37].

Mitochondrial Ca^{2+} retention capacity was estimated using the same assay conditions, with the following exception: calcium chloride was added in pulses of 20 µM until spontaneous release of the ion from the mitochondrial matrix signaled the opening of the MPT pore. The maximum amount of Ca^{2+} supplements absorbed was used to calculate calcium retention capacity and normalized to the amount of mitochondrial protein estimated by the Bradford method (nmol Ca^{2+}/mg protein).

All chemicals mentioned in this section were purchased from Sigma Aldrich (Sigma-Aldrich, St. Louis, MO, USA) unless otherwise stated.

2.7 Statistical Analysis

The data are presented as the mean ± SEM. The statistical significance of the differences between means was calculated using one-way ANOVA followed by Tukey's *post-hoc* test for multiple comparisons using GraphPad Prism 8.0.1 (GraphPad Software Inc., San Diego, CA, USA). A p value of <0.05 was considered statistically significant.

3. Results

3.1 Effect of APB Administration on the Somatic and Biochemical Characteristics of Mice and Skeletal Muscle Health

In this work we used two concentrations of APB: 3 and 10 mg/kg/day. These doses of APB showed positive results in the treatment of Alzheimer's [25] and Parkinson's diseases [24,27], and improved cognitive function in rats subjected to streptozotocin-induced diabetes [38]. *mdx* mice demonstrate a mild phenotype of the disease, without the fibro-fatty progression observed in DMD patients, but associated with decreased muscle strength and endurance. In particular, in our experiment, *mdx* mice exhibited reduced grip strength, wire hanging time, and holding impulse compared to healthy WT animals (Fig. 1). This was accompanied by a significant increase in the activity of creatine kinase, AST and LDH enzymes in the blood serum of dystrophin-deficient animals indicating the disruption of muscle fiber membranes (Fig. 2). In addition, the quadriceps of *mdx* mice showed significant increase in centrally nucleated fibers, total central nuclei, degenerating and regenerating fibers, and inflammation (Fig. 3A and Table 1). We also noted a decrease in the mean minimal Feret's di-

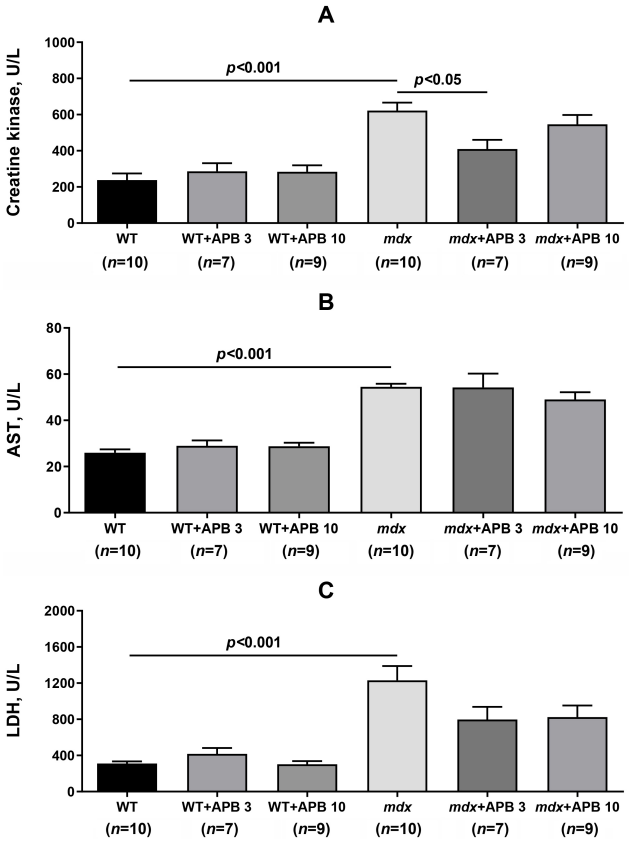

Fig. 2. The effect of APB treatment on the level of enzymes in the blood serum of mice. (A) Creatine kinase. (B) Aspartate aminotransferase (AST). (C) Lactate dehydrogenase (LDH). Data are expressed as mean ± SEM.

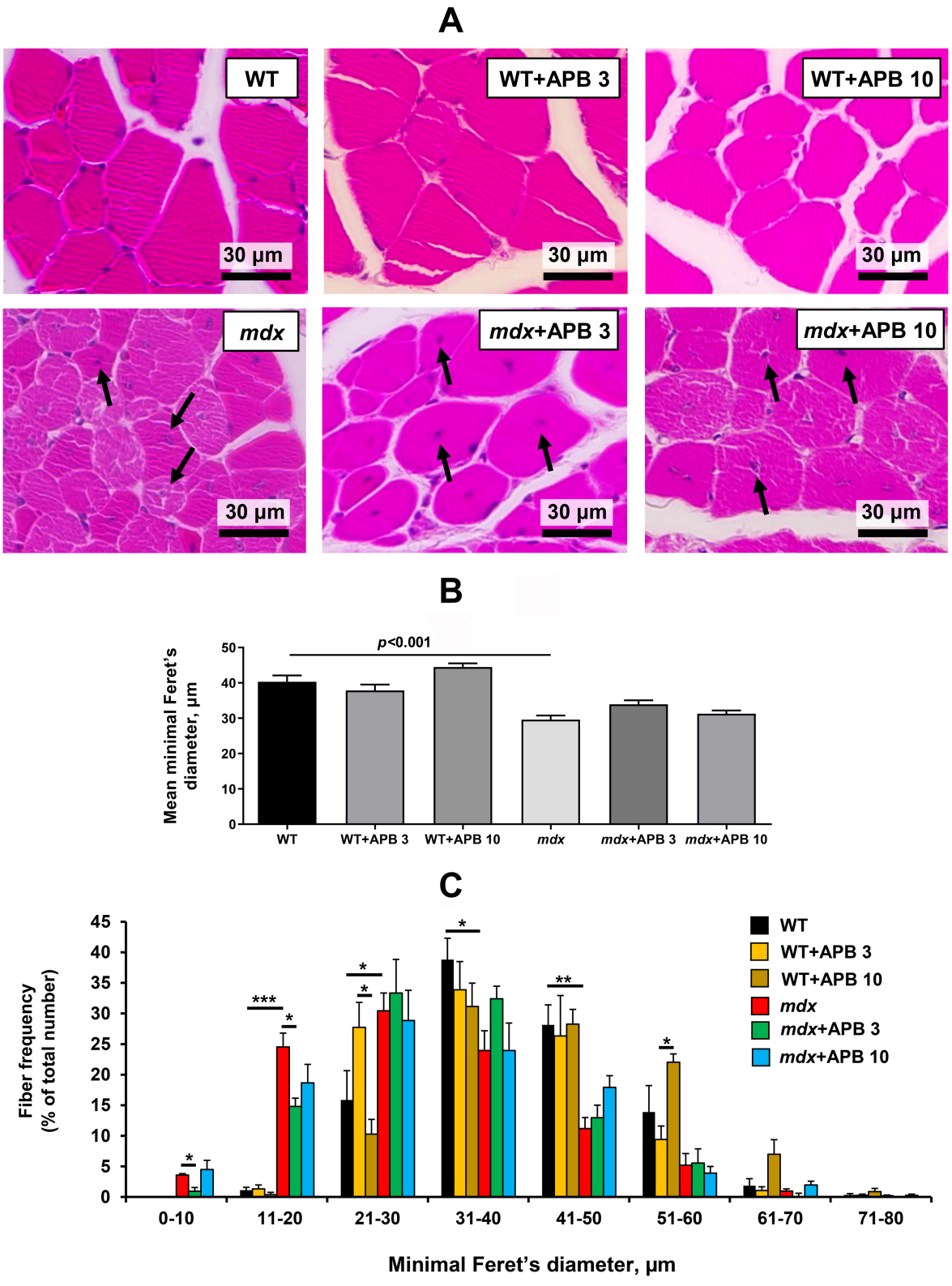

Fig. 3. The effect of APB treatment on histological changes in mouse quadriceps. (A) Representative images of hematoxylin and eosin (H&E) stained cross-sections of mouse quadriceps muscles. Scale bar is 30 µm. Black arrows indicate some centrally located muscle fiber nuclei. (B) Mean minimal Feret's diameter. (C) Fiber size distribution. Data are expressed as mean ± SEM ($n = 5$). * $p < 0.05$, ** $p < 0.01$, *** $p < 0.001$.

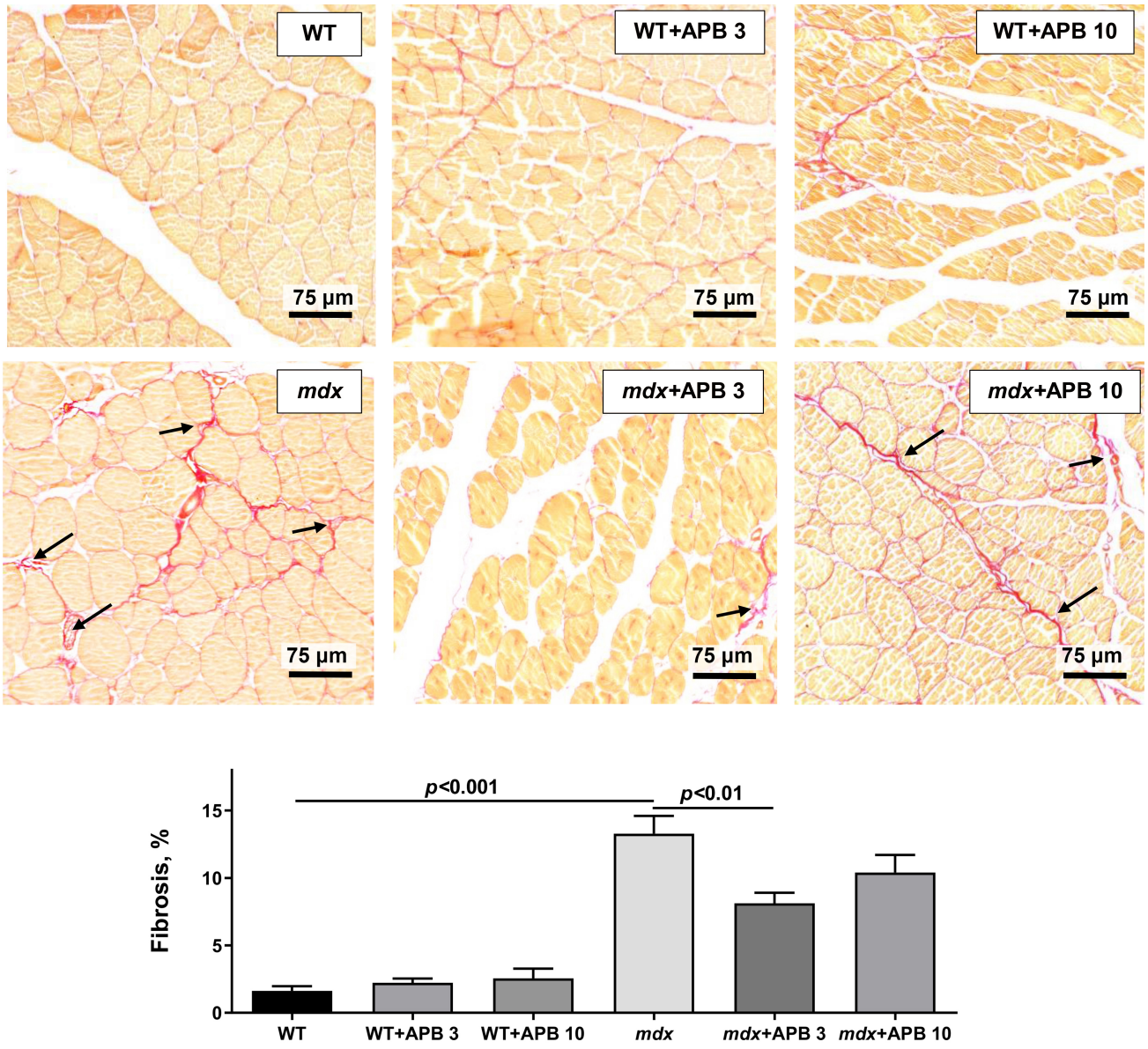

Fig. 4. Representative images of Sirius red stained cross-sections of mouse quadriceps muscles. Scale bar is 75 µm. Black arrows indicate fibrotic regions. The diagram shows the percentage of fibrosis in the quadriceps. Data are expressed as mean ± SEM (n = 5).

ameter of quadriceps muscle fibers in *mdx* mice compared to WT mice due to an increase in the proportion of small fibers (less than 30 µm in diameter) (Fig. 3B,C) corresponding to regenerating fibers. Activation of degeneration and regeneration cycles was also accompanied by an increase in the deposition of connective tissue in the quadriceps of *mdx* mice, which corresponds to the development of fibrosis (Fig. 4).

APB at a concentration of 3 mg/kg significantly reduced the level of creatine kinase in the blood serum of *mdx* mice (Fig. 2), which may reflect the preservation of the integrity of the membranes of some muscle fibers. At the same time, the level of other enzymes (AST and LDH) did not change, although the level of LDH in APB-treated *mdx* mice tended to decrease. Fig. 3 and Table 1 show that 3 mg/kg APB caused a decrease in centrally nucleated fibers, total central and peripheral nuclei, degenerating fibers and inflammation in the quadriceps of *mdx* mice. The mean minimal Feret's diameter of quadriceps muscle fibers in APB-treated *mdx* mice did not change (Fig. 3B). However, 3 mg/kg APB caused a slight rightward shift in the distribution of myofiber sizes in the quadriceps of *mdx* mice due to a significant decrease in the proportion of fibers less than 20 µm in diameter (Fig. 3C), which may indicate a mitigation of the degeneration of dystrophin-deficient fibers. This effect of 3 mg/kg APB was also accompanied by a statistically significant decrease in the level of fibrosis in the quadriceps of *mdx* mice (Fig. 4). However, these events were not sufficient to improve grip strength and hanging time of *mdx* mice (Fig. 1). A high dose of APB (10 mg/kg) had no effect on

the muscle strength of *mdx* mice (Fig. 1), serum enzyme levels (Fig. 2) and fiber size (Fig. 3). At the same time, histological measurements of H&E-stained quadriceps sections showed a reduction in degenerating fibers and inflammatory foci in the quadriceps of *mdx* mice, but the effect was less pronounced than in the case of administration of 3 mg/kg APB. The effect of 10 mg/kg APB was also accompanied by a significant increase in the level of regenerating fibers (Table 1) and a slight tendency to reduce fibrosis in the quadriceps of *mdx* mice (Fig. 4). We noted some negative effects of 10 mg/kg APB on muscle health in WT mice. In particular, this dose of APB caused a statistically significant decrease in grip strength of WT mice and showed a tendency to decrease wire-hanging time and holding impulse of these animals (p = 0.4 *vs.* WT in both cases) (Fig. 1), although we did not detect changes in serum enzyme levels (Fig. 2) and significant morphological changes (Figs. 3,4, Table 1). One should also note that both WT and *mdx* mice treated with 10 mg/kg APB showed a tendency towards a decrease in body weight in the last week of the experiment (Fig. 5).

3.2 Effect of APB Administration on the Ultrastructure of Skeletal Muscles

Skeletal muscles of *mdx* mice, as well as biopsies from DMD patients, are known to show significant ultrastructural abnormalities. Fig. 6 and **Supplementary Fig. 1** show electron microscopic images of the quadriceps of the experimental groups of mice. The quadriceps of healthy WT mice had normal architecture. The bands were clear and the myofilaments were aligned with each other. The sarcoplasmic reticulum was represented mainly by small flattened cisterns. Subsarcolemmal mitochondria, located on the periphery of the muscle fiber, formed large clusters and had a spherical or elongated shape. We did not observe structural disturbances in the cristae or damage to the outer and inner mitochondrial membranes.

The WT+APB 3 and WT+APB 10 groups showed enlarged spaces between myofibrils containing dilated and swollen sarcoplasmic reticulum cisterns surrounding the mitochondria. This was accompanied by a dose-dependent increase in SR/mitochondrion contact area in the quadriceps of WT mice (Fig. 7A). We also noted a decrease in the number of subsarcolemmal mitochondria in the quadriceps of WT+APB 10 mice (Fig. 7B). However, the size of the mitochondria did not change (Fig. 7C).

The *mdx*, *mdx*+APB 3 and *mdx*+APB 10 groups demonstrated similar destructive changes in the ultrastructure of the quadriceps, usually of a local nature and detected in certain areas of the muscle fiber adjacent to the unchanged areas. The sarcomeres had changes in organization. In particular, the Z-disk was often positioned obliquely relative to the longitudinal axis of the fiber and was sometimes interrupted. Myofilaments lost their precise orientation due to rupture of myofibrils. Myofibril diameter is often thinned without disrupting sarcomere organization. Destructive changes were also found in the sarcoplasm, sarcoplasmic reticulum and mitochondria. The spaces of sarcoplasm between myofibrils were greatly expanded. The sarcoplasm showed increased glycogen and secondary lysosome content, as well as proliferation and expansion of the SR cisternae surrounding the mitochondria. Subsarcolemmal mitochondria in the quadriceps of *mdx* mice formed numerous clusters. These areas contained enlarged, swollen, and dilated sarcoplasmic reticulum cisterns that occupied most of the subsarcolemmal space. Mitochondria were predominantly spherical in shape and their diameter was approximately 1.6-fold smaller than that of the WT group (Fig. 7C). Normal mitochondria alternated with mitochondria with destroyed cristae and areas of sharp matrix clearing. The outer membrane of some mitochondria had cracks and ruptures.

Quadriceps muscle of *mdx*+APB 10 mice exhibited few mitochondrial clusters under the sarcolemma. How-

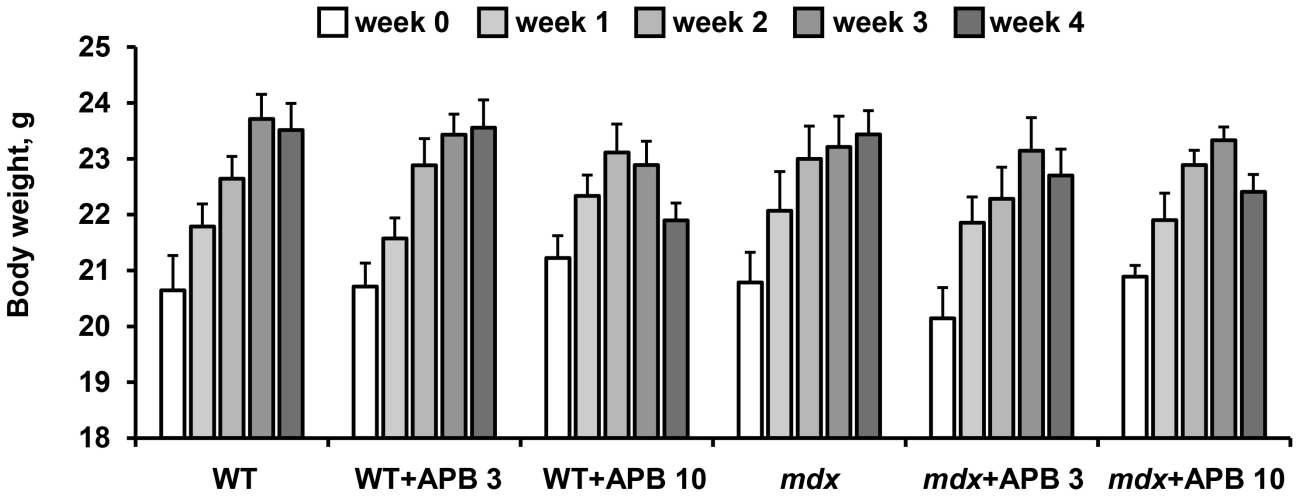

Fig. 5. The effect of APB treatment on body weight gain in experimental groups of mice. Data are expressed as mean ± SEM.

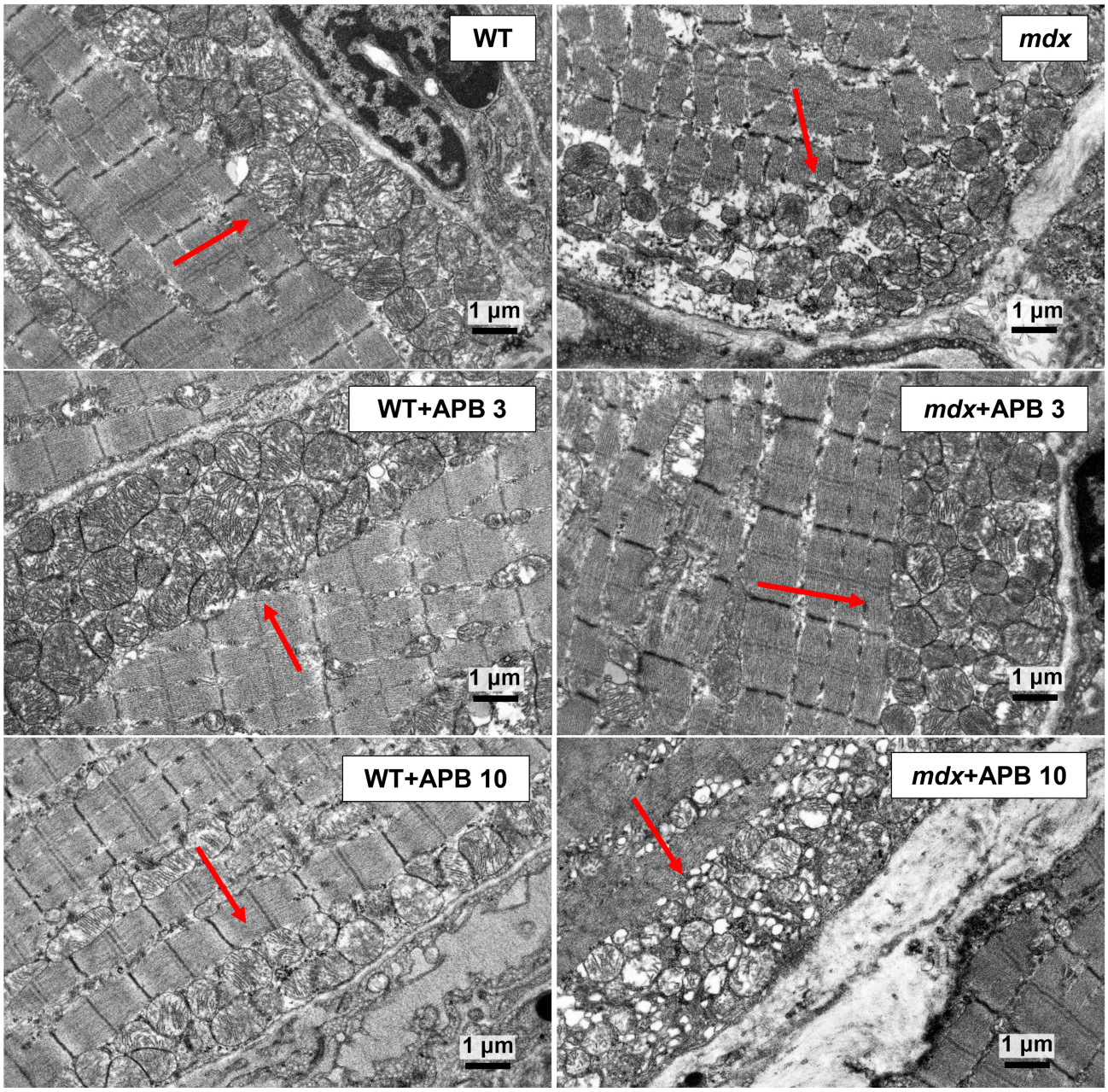

Fig. 6. Representative transmission electron micrographs of mouse quadriceps sections. Mitochondria of the subsarcolemmal population are highlighted with red arrows. Scale bar is 1 µm. High magnification images of subsarcolemmal mitochondria are shown in **Supplementary Fig. 1**.

ever, the *mdx*+APB 3 group did not differ from the WT and *mdx* groups in the number of mitochondria (Fig. 7B). The quadriceps of *mdx* mice treated with 10 mg/kg APB showed the most pronounced destructive changes. The muscle mitochondria in these animals were at different stages of destructive changes: from swelling, compaction of their internal space, deformation and fragmentation of the cristae to ruptures of the outer membrane. The sarcoplasmic reticulum was significantly hypertrophied and this was accompanied by an increase in the area of SR/mitochondrion contacts. However, low concentration of APB (*mdx*+APB 3 group) did not aggravate muscle dystrophy. Moreover, 3 mg/kg APB promoted a decrease in the SR/mitochondrion contact area (Fig. 7A), a phenomenon previously considered as evidence of improvement in both mitochondrial and cellular calcium homeostasis [30].

3.3 Effects of APB Administration on the Functioning of Skeletal Muscle Mitochondria

Ultrastructural abnormalities in dystrophin-deficient muscles are known to be accompanied by the development of mitochondrial dysfunction. This is expressed in the suppression of oxidative phosphorylation, an increase in ROS production and a decrease in the resistance of mitochon-

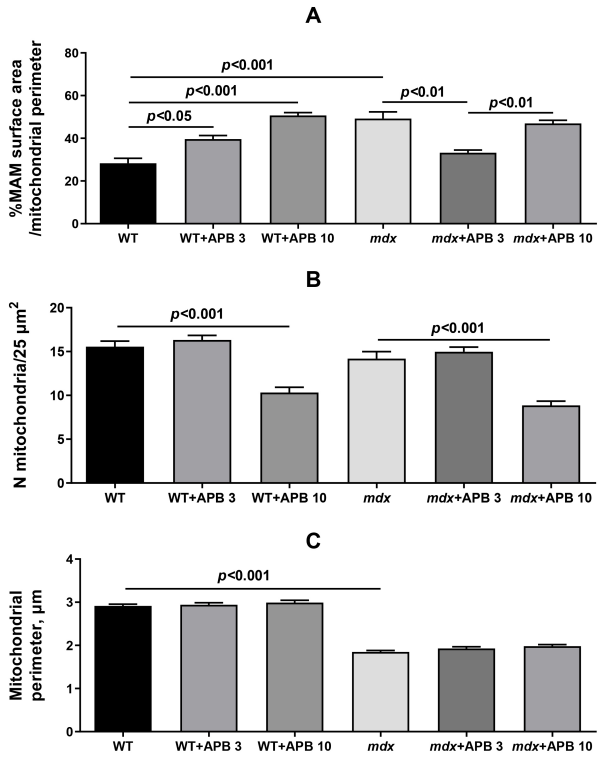

Fig. 7. Electron micrograph (Fig. 6) profiles. (A) Percentage of mitochondria-associated membranes (MAM) surface area per mitochondrion perimeter in each microscopic field. (B) Number of mitochondria per plate. (C) Mitochondrial perimeter. Data are expressed as mean ± SEM (n = 3).

dria to MPT pore opening. All these events contribute to the development of skeletal muscle pathology, including in *mdx* mice [3]. It has previously been shown that reducing Ca^{2+} overload in dystrophin-deficient muscles is also accompanied by improved mitochondrial health [39]. In this work we compared the functional state of skeletal muscle mitochondria isolated from APB treated mice and control animals.

Fig. 8 shows typical polarographic curves demonstrating oxygen consumption by mitochondria isolated from mouse quadriceps. Data reflecting the efficiency of respiration and oxidative phosphorylation in quadriceps mitochondria are summarized in Table 2. Mitochondria isolated from the quadriceps of *mdx* mice exhibited a reduction in state 3 respiration rate (ADP-stimulated) as well as maximal respiration rate in the presence of the protonophore uncoupler 2,4-DNP ($3U_{DNP}$ state) compared to WT animals. These changes were also accompanied by a decrease in the respiratory control ratio (RCR), indicating mitochondrial coupling of respiration to phosphorylation and organelle quality. APB at both tested concentrations had no effect on the studied parameters of mitochondrial respiration in both WT and *mdx* mice.

One of the triggers for the destruction of skeletal muscles in DMD is oxidative stress, which is expressed, among other things, in the development of lipid peroxidation in the mitochondria [3]. Indeed, mitochondria from *mdx* mice exhibited increased levels of lipid peroxidation products (mainly malondialdehyde) (Fig. 9). APB at both doses had no effect on this parameter.

DMD is associated with mitochondrial calcium overload and decreased organelle resistance to calcium-dependent MPT pore opening [3,4]. Indeed, addition of the known pore-forming agent alamethicin to isolated quadriceps mitochondria from *mdx* mice resulted in increased absorption of the Ca^{2+}-sensitive dye arsenazo III, indicating the release of Ca^{2+} from the mitochondrial matrix (Fig. 10A,B). No Ca^{2+} release was observed in quadriceps mitochondria from WT mice. This result indicates a state of chronic Ca^{2+} overload in the skeletal muscle mitochondria of *mdx* mice. As a result, the quadriceps mitochondria from *mdx* mice also absorbed smaller amounts of external Ca^{2+} (Fig. 10C). The *mdx*+APB 3 group showed a tendency (p = 0.4 *vs*. *mdx* group) to decrease the amount of Ca^{2+} released from the mitochondrial matrix, which was also accompanied by a tendency (p = 0.2 *vs*. *mdx* group) to increase the calcium retention capacity (CRC), reflecting the ability of skeletal muscle mitochondria of these animals to absorb external Ca^{2+}. At the same time, 10 mg/kg APB, on the contrary, tended to increase (p = 0.3 *vs*. *mdx* group) the Ca^{2+} overload of quadriceps mitochondria in *mdx* mice, accompanied by a tendency (p = 0.3 *vs*. *mdx* group) to a corresponding reduction in CRC. One should note that mitochondria from *mdx* mice treated with 3 mg/kg APB exhibited sta-

Table 2. Respiration of isolated mouse quadriceps mitochondria from control mice and APB-treated animals.

Animals	State 2	State 3	State 4	State $3U_{DNP}$	RCR
	nmol O_2/min per 1 mg of protein				relative units
WT (n = 6)	34.1 ± 1.6	206.7 ± 4.1	37.1 ± 2.1	279.8 ± 6.2	5.7 ± 0.2
WT+APB 3 (n = 4)	34.0 ± 1.2	186.9 ± 7.9	37.2 ± 0.5	280.8 ± 15.7	5.0 ± 0.2
WT+APB 10 (n = 4)	36.6 ± 0.6	189.2 ± 8.4	37.6 ± 0.9	246.8 ± 10.8	5.0 ± 0.3
mdx (n = 6)	33.8 ± 1.6	181.1 ± 5.1*	37.3 ± 1.7	219.8 ± 7.1*	4.9 ± 0.1*
mdx+APB 3 (n = 5)	29.5 ± 1.3	160.1 ± 6.5*	32.4 ± 2.8	213.9 ± 9.5*	5.1 ± 0.5
mdx+APB 10 (n = 6)	35.3 ± 2.3	173.6 ± 7.1*	37.3 ± 1.7	211.4 ± 13*	4.7 ± 0.2*

The data are presented as means ± SEM. * $p < 0.05$ versus WT group. Data are expressed as mean ± SEM. RCR, respiratory control ratio.

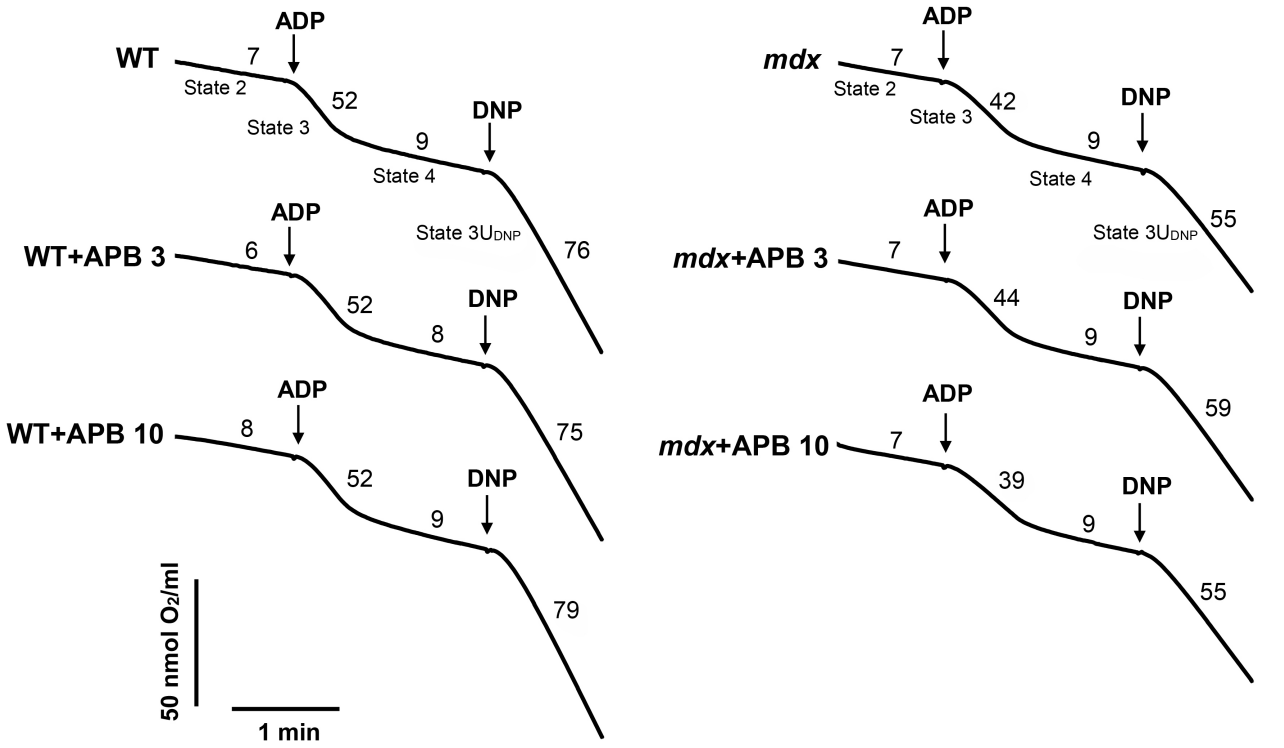

Fig. 8. Typical curves of oxygen consumption by isolated quadriceps mitochondria fueled with glutamate and malate. The numbers adjacent to the curves show the rate of mitochondrial respiration (in nmol O_2/min) in different states. Additions: 200 µM adenosine diphosphate (ADP), 50 µM 2,4-dinitrophenol (DNP). Mitochondrial protein concentration was about 0.25 mg/mL. Data from multiple curves are summarized in Table 2.

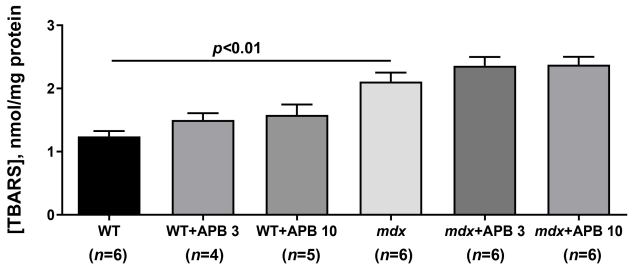

Fig. 9. The effect of APB treatment on lipid peroxidation in mitochondria. Data are expressed as mean ± SEM. TBARS, thiobarbituric acid-reactive substances.

tistically lower calcium overload and, accordingly, higher CRC, compared to mitochondria from *mdx* mice treated with 10 mg/kg APB. In WT mice, APB dose-dependently reduced the CRC of quadriceps mitochondria (Fig. 10C). Moreover, we noted a tendency (p = 0.6 *vs.* WT group) to increase calcium overload of quadriceps mitochondria in mice of the WT+APB 10 group.

4. Discussion

Dysregulation of Ca^{2+} channels in the sarcolemma and intracellular organelles is one of the important secondary consequences of DMD and loss of the dystrophin protein in striated muscles. This event promotes Ca^{2+} overload of muscle fibers, leading to increased activity of Ca^{2+}-dependent proteases and massive proteolysis of cellular proteins, overproduction of ROS and oxidative stress, chronic inflammation, necrosis, inhibition of regenerative capacity and fibrosis [3–5].

In this study, we assessed the effect of intraperitoneal administration of the Ca^{2+} channel modulator APB on the severity of muscle pathology in *mdx* mice. APB has previously been shown to increase the survival of cultured dystrophin-deficient myotubes by eliminating excess cytoplasmic Ca^{2+} overload [28]. The obtained data indicate that APB at a dose of 3 mg/kg body weight also slightly alleviated the muscle pathology in *mdx* mice. This effect was expressed in an improvement in the ultrastructure of the quadriceps muscle (Figs. 6,7) and a decrease in the level of creatine kinase in the blood serum of *mdx* mice (Fig. 2A). 3 mg/kg APB also reduced the number of degenerating fibers and inflammation in the quadriceps of *mdx* mice (Table 1) and this was accompanied by a trend towards an increase in fiber size (Fig. 3) and a statistically significant reduction in fibrosis (Fig. 4). All of this may indicate increased preservation of functional muscle fibers and improved muscle health in *mdx* mice. One could assume that the effect of APB may also be due to some normalization of Ca^{2+} levels in the sarcoplasm of dystrophin-deficient muscles. One

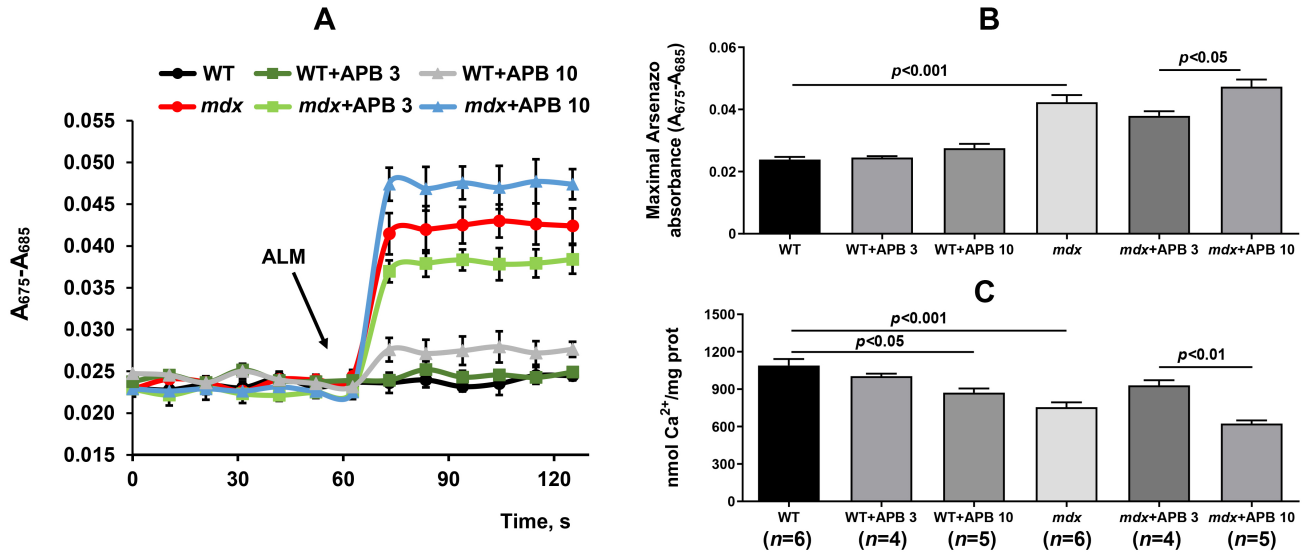

Fig. 10. Effect of APB on mitochondrial Ca^{2+} homeostasis. (A) Mitochondrial Ca^{2+} load assay. 0.1 mg/mL alamethicin (ALM) was added to induce maximal Ca^{2+} release from the mitochondrial matrix. Data are expressed as mean ± SEM (n = 3). (B) Maximal arsenazo absorbance (A_{675}–A_{685}) induced by ALM addition to isolated quadriceps mitochondria. Data are summarized from (A) and expressed as mean ± SEM (n = 3). (C) Calcium retention capacity (CRC) of isolated quadriceps mitochondria assessed by the addition of external Ca^{2+} pulses (per 20 μM). Data are expressed as mean ± SEM.

of the markers of Ca^{2+} overload of muscles in DMD is excessive accumulation of Ca^{2+} in mitochondria [30,40], since under physiological conditions these organelles act only as auxiliary calcium depots, while the main calcium-storing function is assigned to the SR [41,42]. We found that quadriceps mitochondria of *mdx* mice treated with 3 mg/kg APB tended to decrease Ca^{2+} overload (Fig. 10). Furthermore, electron microscopy data show that 3 mg/kg APB promoted a decrease in the area of SR/mitochondrion contact interactions (Fig. 7A), which may also reflect improved Ca^{2+} homeostasis in dystrophin-deficient muscle fibers of *mdx* mice. We have previously observed a similar effect from additional allogeneic mitochondria injected into the skeletal muscles of *mdx* mice, which can act as scavengers of excess Ca^{2+} in pathological tissue [30]. However, the effect of 3 mg/kg APB was insufficient to significantly improve quadriceps mitochondrial function in *mdx* mice. In particular, we did not detect any improvement in either the efficiency of oxidative phosphorylation (Table 2) or the intensity of oxidative stress in *mdx* mice treated with 3 mg/kg APB (Fig. 9). Moreover, this dose of APB failed to improve the impaired muscle strength and endurance of *mdx* mice (Fig. 1).

High dose of APB (10 mg/kg) also had no effect on muscle strength in *mdx* mice (Fig. 1) and showed a less pronounced positive effect on histological parameters in these animals, expressed as a decrease in the level of degenerating fibers and inflammatory foci in the quadriceps (Table 1), but without a statistically significant decrease in the level of fibrosis (Fig. 4). Moreover, electron microscopic images of the quadriceps of *mdx* mice treated with 10 mg/kg APB indicated further worsening of muscle ultrastructure (Figs. 6,7). We also found a trend toward further Ca^{2+} overload of quadriceps mitochondria in *mdx* mice treated with 10 mg/kg APB and a decrease in their ability to accumulate external Ca^{2+} supplements (Fig. 10). All these events may indicate an exacerbation of Ca^{2+} overload in muscle fibers of *mdx* mice. One should note that the aggravation of mitochondrial Ca^{2+} homeostasis in *mdx*+APB 10 mice was particularly evident when compared with the *mdx*+APB 3 group (Fig. 10).

The results obtained indicate that low doses of APB can slow the progression of DMD. However, the effect of APB is not significant even in *mdx* mice exhibiting a relatively mild disease phenotype. The reason for this limited effect of APB may be its well-known multitargeting behavior. Indeed, on the one hand, low concentrations of APB have previously been shown to exert a cytoprotective effect on cultured dystrophin-deficient myotubes by reducing their cytoplasmic calcium overload, apparently due to the inhibition of the overactivated IP_3R pathway of Ca^{2+} release from the SR of dystrophin-deficient muscles and the improvement of the calcium-buffering capacity of the SR [28]. Importantly, recent data have demonstrated that a similar effect can be achieved with the specific pharmacological IP_3R inhibitor xestospongin C, which improved the state of dystrophin-deficient cells by normalizing mitochondrial Ca^{2+} homeostasis and membrane potential [39]. On the other hand, a series of studies by Iwata and colleagues [43,44] showed that high concentrations of APB, on the contrary, promote excessive Ca^{2+} influx from the extracellular space into dystrophin-deficient muscle fibers

through APB-sensitive TRPV2 channels overexpressed in the sarcolemma of *mdx* mice and other model systems, as well as patient biopsies. This may contribute to a further increase in Ca^{2+} levels in dystrophin-deficient muscles and aggravation of the pathology. One should also keep in mind the numerous other targets of APB, including SERCA [7–9], SOCE channels [10–12], TRPC1/3/4/6/7 [13–16], and even mitochondrial electron transport chain complexes [19]. Perhaps this is why the complex multicellular organism of *mdx* mice, demonstrating differential expression of APB-sensitive proteins, also showed an ambiguous response to APB administration. It is important to note that APB had no effect on elevated serum AST levels in *mdx* mice, which is both a marker of heart muscle injury typical of DMD [45] and liver damage described in a number of cases [46]. This may indicate a limited effect of APB only on the skeletal muscles of *mdx* mice. However, this phenomenon requires further study of the effects of APB on other tissues, including non-muscle tissues and other skeletal muscle groups, such as the diaphragm, which is most susceptible to destructive changes in *mdx* mice [47].

One could also assume that multitargeting feature of APB also caused the dysregulation of Ca^{2+} homeostasis in the quadriceps of WT mice. This assumption may be indirectly supported by the decreased Ca^{2+}-buffering capacity of quadriceps mitochondria from WT mice treated with 10 mg/kg APB, as well as significant disruption of the ultrastructure of mitochondria, SR, their contact interactions, and skeletal muscles as a whole. All these events were accompanied by a reduction in muscle function in these animals.

5. Conclusions

The calcium channel modulator APB has previously been shown to improve the survival of cultured dystrophin-deficient myotubes [28]. Our results demonstrate that intraperitoneally administered APB also has the ability to ameliorate the disease phenotype in the dystrophin-deficient *mdx* mouse model. However, the effect of APB is quite limited, possibly due to its known multitargeting behavior. This problem may be addressed by the combined use of APB and other Ca^{2+} transport modulators, such as ryanodine receptor inhibitors, which may result in the suppression of both IP_3R- and RyR-mediated Ca^{2+} release from the sarcoplasmic reticulum into the cytoplasm and prevent its Ca^{2+} overload. It is also possible to design more selective APB analogues that can effectively prevent or at least reduce Ca^{2+} overload of muscle fibers.

Abbreviations

APB, 2-aminoethoxydiphenyl borate; AST, aspartate aminotransferase; DMD, Duchenne muscular dystrophy; IP_3R, inositol-1,4,5-triphosphate receptor; LDH, lactate dehydrogenase; MPT, mitochondrial permeability transition; SR, sarcoplasmic reticulum; WT, wild type.

Availability of Data and Materials

The datasets used and/or analyzed during the current study are available from the corresponding author on reasonable request.

Author Contributions

MVD designed the research study. MVD, AES, ADI, IBM, EYT, AAC and KNB performed the research. MVD, IBM and KNB analyzed the data. MVD wrote the manuscript. All authors contributed to editorial changes in the manuscript. All authors read and approved the final manuscript. All authors have participated sufficiently in the work and agreed to be accountable for all aspects of the work.

Ethics Approval and Consent to Participate

The study with mice was in line with the European Convention for the Protection of Vertebrates used for experimental and other purposes (Strasbourg, 1986). The research protocol was approved by the Mari State University Ethics Committee (protocol No. 01/2023 of 30.11.2023).

Acknowledgment

The authors acknowledge Moscow State University development program (PNR 5.13) and "Superresolution microscopy and spectroscopy" core facility at Belozersky Institute of Physico-chemical biology for granting the access to their equipment.

Funding

This work was supported by grant from the Russian Science Foundation (23-75-10006, https://rscf.ru/project/23-75-10006/).

Conflict of Interest

The authors declare no conflict of interest. Given his role as the Guest Editor, Mikhail V. Dubinin had no involvement in the peer-review of this article and has no access to information regarding its peer review. Full responsibility for the editorial process for this article was delegated to Ioanna-Katerina Aggeli.

Supplementary Material

Supplementary material associated with this article can be found, in the online version, at https://doi.org/10.31083/j.fbl2912428.

References

[1] Monaco AP, Neve RL, Colletti-Feener C, Bertelson CJ, Kurnit DM, Kunkel LM. Isolation of candidate cDNAs for portions of the Duchenne muscular dystrophy gene. Nature. 1986; 323: 646–650. https://doi.org/10.1038/323646a0.

[2] Duan D, Goemans N, Takeda S, Mercuri E, Aartsma-Rus A. Duchenne muscular dystrophy. Nature Reviews.

Disease Primers. 2021; 7: 13. https://doi.org/10.1038/s41572-021-00248-3.

[3] Dubinin MV, Belosludtsev KN. Ion Channels of the Sarcolemma and Intracellular Organelles in Duchenne Muscular Dystrophy: A Role in the Dysregulation of Ion Homeostasis and a Possible Target for Therapy. International Journal of Molecular Sciences. 2023; 24: 2229. https://doi.org/10.3390/ijms24032229.

[4] Mareedu S, Million ED, Duan D, Babu GJ. Abnormal Calcium Handling in Duchenne Muscular Dystrophy: Mechanisms and Potential Therapies. Frontiers in Physiology. 2021; 12: 647010. https://doi.org/10.3389/fphys.2021.647010.

[5] Leyva-Leyva M, Sandoval A, Felix R, González-Ramírez R. Biochemical and Functional Interplay Between Ion Channels and the Components of the Dystrophin-Associated Glycoprotein Complex. The Journal of Membrane Biology. 2018; 251: 535–550. https://doi.org/10.1007/s00232-018-0036-9.

[6] Maruyama T, Kanaji T, Nakade S, Kanno T, Mikoshiba K. 2APB, 2-aminoethoxydiphenyl borate, a membrane-penetrable modulator of Ins(1,4,5)P3-induced Ca2+ release. Journal of Biochemistry. 1997; 122: 498–505. https://doi.org/10.1093/oxfordjournals.jbchem.a021780.

[7] Bilmen JG, Wootton LL, Godfrey RE, Smart OS, Michelangeli F. Inhibition of SERCA Ca2+ pumps by 2-aminoethoxydiphenyl borate (2-APB). 2-APB reduces both Ca2+ binding and phosphoryl transfer from ATP, by interfering with the pathway leading to the Ca2+-binding sites. European Journal of Biochemistry. 2002; 269: 3678–3687. https://doi.org/10.1046/j.1432-1033.2002.03060.x.

[8] Missiaen L, Callewaert G, De Smedt H, Parys JB. 2-Aminoethoxydiphenyl borate affects the inositol 1,4,5-trisphosphate receptor, the intracellular Ca2+ pump and the non-specific Ca2+ leak from the non-mitochondrial Ca2+ stores in permeabilized A7r5 cells. Cell Calcium. 2001; 29: 111–116. https://doi.org/10.1054/ceca.2000.0163.

[9] Peppiatt CM, Collins TJ, Mackenzie L, Conway SJ, Holmes AB, Bootman MD, *et al*. 2-Aminoethoxydiphenyl borate (2-APB) antagonises inositol 1,4,5-trisphosphate-induced calcium release, inhibits calcium pumps and has a use-dependent and slowly reversible action on store-operated calcium entry channels. Cell Calcium. 2003; 34: 97–108. https://doi.org/10.1016/s0143-4160(03)00026-5.

[10] Dellis O, Mercier P, Chomienne C. The boron-oxygen core of borinate esters is responsible for the store-operated calcium entry potentiation ability. BMC Pharmacology. 2011; 11: 1. https://doi.org/10.1186/1471-2210-11-1.

[11] Peinelt C, Lis A, Beck A, Fleig A, Penner R. 2-Aminoethoxydiphenyl borate directly facilitates and indirectly inhibits STIM1-dependent gating of CRAC channels. The Journal of Physiology. 2008; 586: 3061–3073. https://doi.org/10.1113/jphysiol.2008.151365.

[12] Wei M, Zhou Y, Sun A, Ma G, He L, Zhou L, *et al*. Molecular mechanisms underlying inhibition of STIM1-Orai1-mediated Ca^{2+} entry induced by 2-aminoethoxydiphenyl borate. Pflugers Archiv: European Journal of Physiology. 2016; 468: 2061–2074. https://doi.org/10.1007/s00424-016-1880-z.

[13] Lievremont JP, Bird GS, Putney JW, Jr. Mechanism of inhibition of TRPC cation channels by 2-aminoethoxydiphenylborane. Molecular Pharmacology. 2005; 68: 758–762. https://doi.org/10.1124/mol.105.012856.

[14] Clapham DE. Calcium signaling. Cell. 2007; 131: 1047–1058. https://doi.org/10.1016/j.cell.2007.11.028.

[15] Chokshi R, Fruasaha P, Kozak JA. 2-aminoethyl diphenyl borinate (2-APB) inhibits TRPM7 channels through an intracellular acidification mechanism. Channels. 2012; 6: 362–369. https://doi.org/10.4161/chan.21628.

[16] Malko P, Syed Mortadza SA, McWilliam J, Jiang LH. TRPM2 Channel in Microglia as a New Player in Neuroinflammation Associated With a Spectrum of Central Nervous System Pathologies. Frontiers in Pharmacology. 2019; 10: 239. https://doi.org/10.3389/fphar.2019.00239.

[17] Knox CD, Belous AE, Pierce JM, Wakata A, Nicoud IB, Anderson CD, *et al*. Novel role of phospholipase C-delta1: regulation of liver mitochondrial Ca2+ uptake. American Journal of Physiology. Gastrointestinal and Liver Physiology. 2004; 287: G533–40. https://doi.org/10.1152/ajpgi.00050.2004.

[18] Nicoud IB, Knox CD, Jones CM, Anderson CD, Pierce JM, Belous AE, *et al*. 2-APB protects against liver ischemia-reperfusion injury by reducing cellular and mitochondrial calcium uptake. American Journal of Physiology. Gastrointestinal and Liver Physiology. 2007; 293: G623–G630. https://doi.org/10.1152/ajpgi.00521.2006.

[19] Dubinin MV, Chulkov AV, Igoshkina AD, Cherepanova AA, Mikina NV. Effect of 2-aminoethoxydiphenyl borate on the functions of mouse skeletal muscle mitochondria. Biochemical and Biophysical Research Communications. 2024; 712–713: 149944. https://doi.org/10.1016/j.bbrc.2024.149944.

[20] Hu H, Grandl J, Bandell M, Petrus M, Patapoutian A. Two amino acid residues determine 2-APB sensitivity of the ion channels TRPV3 and TRPV4. Proceedings of the National Academy of Sciences of the United States of America. 2009; 106: 1626–1631. https://doi.org/10.1073/pnas.0812209106.

[21] Hu HZ, Gu Q, Wang C, Colton CK, Tang J, Kinoshita-Kawada M, *et al*. 2-aminoethoxydiphenyl borate is a common activator of TRPV1, TRPV2, and TRPV3. The Journal of Biological Chemistry. 2004; 279: 35741–35748. https://doi.org/10.1074/jbc.M404164200.

[22] Kovacs G, Montalbetti N, Simonin A, Danko T, Balazs B, Zsembery A, *et al*. Inhibition of the human epithelial calcium channel TRPV6 by 2-aminoethoxydiphenyl borate (2-APB). Cell Calcium. 2012; 52: 468–480. https://doi.org/10.1016/j.ceca.2012.08.005.

[23] Pumroy RA, Protopopova AD, Fricke TC, Lange IU, Haug FM, Nguyen PT, *et al*. Structural insights into TRPV2 activation by small molecules. Nature Communications. 2022; 13: 2334. https://doi.org/10.1038/s41467-022-30083-3.

[24] Vaidya B, Kaur H, Thapak P, Sharma SS, Singh JN. Pharmacological Modulation of TRPM2 Channels via PARP Pathway Leads to Neuroprotection in MPTP-induced Parkinson's Disease in Sprague Dawley Rats. Molecular Neurobiology. 2022; 59: 1528–1542. https://doi.org/10.1007/s12035-021-02711-4.

[25] Thapak P, Khare P, Bishnoi M, Sharma SS. Neuroprotective Effect of 2-Aminoethoxydiphenyl Borate (2-APB) in Amyloid β-Induced Memory Dysfunction: A Mechanistic Study. Cellular and Molecular Neurobiology. 2022; 42: 1211–1223. https://doi.org/10.1007/s10571-020-01012-z.

[26] Morihara H, Obana M, Tanaka S, Kawakatsu I, Tsuchiyama D, Mori S, *et al*. 2-aminoethoxydiphenyl borate provides an antioxidative effect and mediates cardioprotection during ischemia reperfusion in mice. PLoS ONE. 2017; 12: e0189948. https://doi.org/10.1371/journal.pone.0189948.

[27] Vaidya B, Polepalli M, Sharma SS, Singh JN. 2-Aminoethoxydiphenyl borate ameliorates mitochondrial dysfunctions in MPTP/MPP^+ model of Parkinson's disease. Mitochondrion. 2023; 69: 95–103. https://doi.org/10.1016/j.mito.2023.02.003.

[28] Mondin L, Balghi H, Constantin B, Cognard C, Sebille S. Negative modulation of inositol 1,4,5-trisphosphate type 1 receptor expression prevents dystrophin-deficient muscle cells death. American Journal of Physiology. Cell Physiology. 2009; 297: C1133–C1145. https://doi.org/10.1152/ajpcell.00048.2009.

[29] van Putten M, Aartsma-Rus A, Louvain-la-Neuve L. The use of hanging wire tests to monitor muscle strength and condition over

time. Treat-Nmd.Eu. 2012; 1–12.

[30] Dubinin MV, Mikheeva IB, Stepanova AE, Igoshkina AD, Cherepanova AA, Semenova AA, *et al*. Mitochondrial Transplantation Therapy Ameliorates Muscular Dystrophy in *mdx* Mouse Model. Biomolecules. 2024; 14: 316. https://doi.org/10.3390/biom14030316.

[31] Kumar A, Accorsi A, Rhee Y, Girgenrath M. Do's and don'ts in the preparation of muscle cryosections for histological analysis. Journal of Visualized Experiments. 2015; e52793. https://doi.org/10.3791/52793.

[32] Spurney CF, Gordish-Dressman H, Guerron AD, Sali A, Pandey GS, Rawat R, *et al*. Preclinical drug trials in the mdx mouse: assessment of reliable and sensitive outcome measures. Muscle & Nerve. 2009; 39: 591–602. https://doi.org/10.1002/mus.21211.

[33] Dubinin MV, Starinets VS, Belosludtseva NV, Mikheeva IB, Chelyadnikova YA, Igoshkina AD, *et al*. BK_{Ca} Activator NS1619 Improves the Structure and Function of Skeletal Muscle Mitochondria in Duchenne Dystrophy. Pharmaceutics. 2022; 14: 2336. https://doi.org/10.3390/pharmaceutics14112336.

[34] Thoudam T, Ha CM, Leem J, Chanda D, Park JS, Kim HJ, *et al*. PDK4 Augments ER-Mitochondria Contact to Dampen Skeletal Muscle Insulin Signaling During Obesity. Diabetes. 2019; 68: 571–586. https://doi.org/10.2337/db18-0363.

[35] Frezza C, Cipolat S, Scorrano L. Organelle isolation: functional mitochondria from mouse liver, muscle and cultured fibroblasts. Nature Protocols. 2007; 2: 287–295. https://doi.org/10.1038/nprot.2006.478.

[36] CHANCE B, WILLIAMS GR. Respiratory enzymes in oxidative phosphorylation. I. Kinetics of oxygen utilization. The Journal of Biological Chemistry. 1955; 217: 383–393.

[37] Bround MJ, Havens JR, York AJ, Sargent MA, Karch J, Molkentin JD. ANT-dependent MPTP underlies necrotic myofiber death in muscular dystrophy. Science Advances. 2023; 9: eadi2767. https://doi.org/10.1126/sciadv.adi2767.

[38] Thapak P, Bishnoi M, Sharma SS. Pharmacological Inhibition of Transient Receptor Potential Melastatin 2 (TRPM2) Channels Attenuates Diabetes-induced Cognitive Deficits in Rats: A Mechanistic Study. Current Neurovascular Research. 2020; 17: 249–258. https://doi.org/10.2174/1567202617666200415142211.

[39] Valladares D, Utreras-Mendoza Y, Campos C, Morales C, Diaz-Vegas A, Contreras-Ferrat A, *et al*. IP_3 receptor blockade restores autophagy and mitochondrial function in skeletal muscle fibers of dystrophic mice. Biochimica et Biophysica Acta. Molecular Basis of Disease. 2018; 1864: 3685–3695. https://doi.org/10.1016/j.bbadis.2018.08.042.

[40] Dubinin MV, Stepanova AE, Mikheeva IB, Igoshkina AD, Cherepanova AA, Talanov EY, *et al*. Reduction of Mitochondrial Calcium Overload via MKT077-Induced Inhibition of Glucose-Regulated Protein 75 Alleviates Skeletal Muscle Pathology in Dystrophin-Deficient mdx Mice. International Journal of Molecular Sciences. 2024; 25: 9892. https://doi.org/10.3390/ijms25189892.

[41] Periasamy M, Kalyanasundaram A. SERCA pump isoforms: their role in calcium transport and disease. Muscle & Nerve. 2007; 35: 430–442. https://doi.org/10.1002/mus.20745.

[42] Tupling AR. The decay phase of Ca2+ transients in skeletal muscle: regulation and physiology. Applied Physiology, Nutrition, and Metabolism. 2009; 34: 373–376. https://doi.org/10.1139/H09-033.

[43] Iwata Y, Katanosaka Y, Arai Y, Komamura K, Miyatake K, Shigekawa M. A novel mechanism of myocyte degeneration involving the Ca2+-permeable growth factor-regulated channel. The Journal of Cell Biology. 2003; 161: 957–967. https://doi.org/10.1083/jcb.200301101.

[44] Iwata Y, Katanosaka Y, Arai Y, Shigekawa M, Wakabayashi S. Dominant-negative inhibition of Ca2+ influx via TRPV2 ameliorates muscular dystrophy in animal models. Human Molecular Genetics. 2009; 18: 824–834. https://doi.org/10.1093/hmg/ddn408.

[45] Liu X, Yao S, Pan M, Cai Y, Shentu W, Cai W, *et al*. Two-dimensional speckle tracking echocardiography demonstrates improved myocardial function after intravenous infusion of bone marrow mesenchymal stem in the X-Linked muscular dystrophy mice. BMC Cardiovascular Disorders. 2022; 22: 461. https://doi.org/10.1186/s12872-022-02886-1.

[46] Naume MM, Jørgensen MH, Høi-Hansen CE, Born AP, Vissing J, Borgwardt L, *et al*. Metabolic assessment in children with neuromuscular disorders shows risk of liver enlargement, steatosis and fibrosis. Acta Paediatrica. 2023; 112: 846–853. https://doi.org/10.1111/apa.16649.

[47] Stedman HH, Sweeney HL, Shrager JB, Maguire HC, Panettieri RA, Petrof B, *et al*. The mdx mouse diaphragm reproduces the degenerative changes of Duchenne muscular dystrophy. Nature. 1991; 352: 536–539. https://doi.org/10.1038/352536a0.